Title
A comprehensive formulation for volumetric modulated arc therapy planning.

Journal
Medical physics, 43(7)

ISSN
0094-2405

Authors
Nguyen, Dan
Lyu, Qihui
Ruan, Dan
et al.

Publication Date
2016-07-01

DOI
10.1118/1.4953832

Peer reviewed

A comprehensive formulation for volumetric modulated arc therapy planning

Dan Nguyen, Qihui Lyu, Dan Ruan, Daniel O'Connor, Daniel A. Low, and Ke Sheng[a)]
Department of Radiation Oncology, University of California Los Angeles, Los Angeles, California 90024

(Received 23 February 2016; revised 11 May 2016; accepted for publication 1 June 2016; published 15 June 2016)

Purpose: Volumetric modulated arc therapy (VMAT) is a widely employed radiation therapy technique, showing comparable dosimetry to static beam intensity modulated radiation therapy (IMRT) with reduced monitor units and treatment time. However, the current VMAT optimization has various greedy heuristics employed for an empirical solution, which jeopardizes plan consistency and quality. The authors introduce a novel direct aperture optimization method for VMAT to overcome these limitations.

Methods: The comprehensive VMAT (comVMAT) planning was formulated as an optimization problem with an L2-norm fidelity term to penalize the difference between the optimized dose and the prescribed dose, as well as an anisotropic total variation term to promote piecewise continuity in the fluence maps, preparing it for direct aperture optimization. A level set function was used to describe the aperture shapes and the difference between aperture shapes at adjacent angles was penalized to control MLC motion range. A proximal-class optimization solver was adopted to solve the large scale optimization problem, and an alternating optimization strategy was implemented to solve the fluence intensity and aperture shapes simultaneously. Single arc comVMAT plans, utilizing 180 beams with 2° angular resolution, were generated for a glioblastoma multiforme case, a lung (LNG) case, and two head and neck cases—one with three PTVs ($H\&N_{3PTV}$) and one with foue PTVs ($H\&N_{4PTV}$)—to test the efficacy. The plans were optimized using an alternating optimization strategy. The plans were compared against the clinical VMAT (clnVMAT) plans utilizing two overlapping coplanar arcs for treatment.

Results: The optimization of the comVMAT plans had converged within 600 iterations of the block minimization algorithm. comVMAT plans were able to consistently reduce the dose to all organs-at-risk (OARs) as compared to the clnVMAT plans. On average, comVMAT plans reduced the max and mean OAR dose by 6.59% and 7.45%, respectively, of the prescription dose. Reductions in max dose and mean dose were as high as 14.5 Gy in the LNG case and 15.3 Gy in the $H\&N_{3PTV}$ case. PTV coverages measured by *D*95, *D*98, and *D*99 were within 0.25% of the prescription dose. By comprehensively optimizing all beams, the comVMAT optimizer gained the freedom to allow some selected beams to deliver higher intensities, yielding a dose distribution that resembles a static beam IMRT plan with beam orientation optimization.

Conclusions: The novel nongreedy VMAT approach simultaneously optimizes all beams in an arc and then directly generates deliverable apertures. The single arc VMAT approach thus fully utilizes the digital Linac's capability in dose rate and gantry rotation speed modulation. In practice, the new single VMAT algorithm generates plans superior to existing VMAT algorithms utilizing two arcs.
 [http://dx.doi.org/10.1118/1.4953832]

Key words: volumetric modulated arc therapy, non-greedy, non-heuristic, direct aperture optimization

1. INTRODUCTION

Volumetric modulated arc therapy (VMAT) is a widely adopted radiation therapy technique. The adoption was supported by dosimetric studies showing that with comparable dose distributions,[1] VMAT is significantly more efficient in both treatment time and total monitor units (MU) than static beam intensity modulated radiation therapy (IMRT).[2–4] The theoretical framework of VMAT was originally introduced in 1995 by Yu[5] as intensity modulated arc therapy (IMAT), which generated multiple MLC segments per beam angle and requires multiple arcs to deliver.[6–8] More practical single arc VMAT algorithms were subsequently developed[9–11] including a representative publication by Otto.[12]

Compared to the static beam IMRT problem, the arc optimization problem was considered significantly more complex, due both to the substantially increased beam orientations and the additional machine mechanical constraints such as gantry and MLC mechanical limits. Using a multiresolution approach,[9–12] several methods progressively inserted new beams between sparsely sampled beams using interpolation and then randomly sampled MLC aperture shapes and weights using simulated annealing. These methods were effective to reduce the optimization problem complexity and achieve

aperture continuity between adjacent apertures. However, such greedy methods do not guarantee optimality. To mitigate the local minimum problem, in practice, two or more arcs are still commonly required to introduce different initial conditions and achieve the desired dosimetry,[13] despite the original promise of using the single arc. Also due to the multiresolution approach, optimization weights and penalties applied at earlier stages of optimization tend to carry a greater influence. In addition to the stochastic nature of simulated annealing optimization, the optimization results highly depend on the order and timing that the optimization parameters are applied, making reproducing an existing plan difficult, if not impossible. Craft *et al.*[14] attempted to avoid the progressive sampling issue by starting an IMRT optimization at every 2°, and then created the apertures by merging and simplifying adjacent fluence maps. This leads to another problem that is common in inverse treatment planning, which is the heuristic conversion from fluence map to MLC segments, which typically introduces noticeable and unpredictable dosimetric quality degradations.[15–17]

To avoid the stochastic simulated annealing method used in previous direct aperture VMAT implementations and directly optimize based on beam apertures, Peng *et al.* developed a column-generation-based VMAT method algorithm.[18] This method iteratively selects a new aperture for densely sampled arc beams from an aperture set based on its contribution to the objective function. Once the aperture is selected, the optimization proceeds to the next beam and selects the next aperture, imposing potential mechanical limitations based on the previous aperture shape. This method has obvious limitations from being a greedy heuristic algorithm, as it solves a subproblem in each step that does not simultaneously optimize all possible beam angles. Furthermore, the number of possible aperture shapes increases combinatorially. Using a complete aperture set for large tumor or high resolution dose modulation quickly becomes mathematically intractable. Cheng *et al.* introduced a binary level-set shape optimization model for VMAT, illustrating the efficacy of level-set methods for radiotherapy.[19] While efficient, the disadvantage to using a binary level-set lies in that fact the level-set function is discontinuous. Derivatives of the level-set at the boundary do not exist and this can lead to poor accuracy in the variational approach. Because of the pivotal role of VMAT in today's radiotherapy practice, there is a strong need to overcome the existing limitations and develop a new level-set based VMAT framework that formulates the full DAO program using a continuous level-set function.

2. MATERIALS AND METHODS

2.A. Optimization formulation

The proposed comprehensive VMAT (comVMAT) optimization formulation takes the following form:

$$\begin{aligned}
&\underset{\{f_\theta, c_\theta, \Phi_\theta\}_{\theta=0}^{n}}{\operatorname{argmin}} \underbrace{\frac{1}{2}\left\| W\left(\sum_\theta (A_\theta f_\theta) - d_0\right)\right\|_2^2}_{\text{dose fidelity term}} + \sum_\theta \underbrace{(\lambda_1 \|D_{1\theta} f_\theta\|_1 + \lambda_2 \|D_{2\theta} f_\theta\|_1)}_{\text{term set 1}} \\
&+ \sum_\theta \sum_{x,y} \Bigg(\underbrace{\frac{\gamma}{2}\left[(f_{\theta xy} - c_\theta)^2 H(\Phi_\theta(x,y)) + f_{\theta xy}^2 (1 - H(\Phi_\theta(x,y)))\right]}_{\text{term set 2}} \\
&+ \underbrace{\frac{k}{2}\left[(H(\Phi_\theta(x,y)) - H(\Phi_{\theta-1}(x,y)))^2 + (H(\Phi_\theta(x,y)) - H(\Phi_{\theta+1}(x,y)))^2\right]}_{\text{term set 3}} \Bigg), \\
&\text{subject to } f \geq 0,
\end{aligned} \tag{1}$$

where f_θ, c_θ, and Φ_θ are the optimization variables. f_θ is the vectorized fluence map, c_θ is a value that f approaches within an aperture, and Φ_θ is the level set function,[20] defined as positive where the aperture exists and negative elsewhere. The level set $\{(x,y)|\Phi_\theta(x,y) = 0\}$ describes the aperture boundary. Beam angles are indexed by θ, which ranges from 1 to n, and x and y are indices for a beamlet at a given θ. The fluence to dose transformation matrix is denoted by A, and the desired dose, d_0, is set as the prescription dose at the PTV and zero elsewhere. The diagonal weighting matrix, W, weighs the structures of interest. The derivative matrices, D_1 and D_2, take the derivative of the fluence in both directions parallel and orthogonal to the MLC leaf movement. H is the Heaviside function,

$$H(v) = \begin{cases} 1 & \text{if } v \geq 0 \\ 0 & \text{if } v < 0 \end{cases}. \tag{2}$$

Essentially, $H(\Phi_\theta(x,y))$ equals one inside the aperture and zero elsewhere. $f_{\theta xy}$ is a scalar value representing a single beamlet at a given beam angle θ and an x and y location on the beam, while f_θ is a vector of all the fluences at a specific

beam angles. c_θ is a scalar quantity and only has one value per beam at a given time.

Intuitively, the dose fidelity term, in Eq. (1), attempts to push the final dose as close as possible to the desired dose. Term set 1 is the anisotropic total variation (TV) regularization, which has been shown to successfully encourage piecewise continuity on the fluence maps.[21,22] The TV regularization term considers the entire fluence map of the beam, so the term ultimately controls the segment size and shape, abating irregularities and holes in the aperture shape. Soft regulation of the minimal leaf gap and the max leaf interdigitation can be accomplished by independently adjusting the weightings λ_1 and λ_2, respectively. Term set 2 is pushing f toward c where the aperture is defined and zero elsewhere. Term set 3 encourages adjacent beam angles to be similar to regulate leaf movement between beam angles. For the first and n-th θ, the $\Phi_{\theta-1}(x,y)$ and $\Phi_{\theta+1}(x,y)$ are equal to their respective $\Phi_\theta(x,y)$.

2.B. Algorithm

We use a block minimization algorithm to solve the minimization problem in Eq. (1) by alternatingly updating the fluence f_θ, aperture intensity c_θ, and aperture shape Φ_θ, while holding the other two constant. The algorithm is broken down into 3 modules described below. Each iteration of the algorithm runs module 1 through 3, and the process is repeated until a satisfactory convergence rate is achieved. Convergence of the alternating approach is guaranteed, as long as each module is able to find a minimum for its respective variable, while holding the other variables constant. A proof of the convergence is provided by Gorski *et al.*[23]

2.B.1. Algorithm module 1: Update f_θ

Module 1 minimizes Eq. (1) w.r.t. f_θ while holding c_θ and Φ_θ constant. This subproblem can be rewritten as

$$\begin{aligned}\underset{\{f_\theta\}_{\theta=0}^{n}}{\operatorname{argmin}} \quad & \frac{1}{2}\left\| W\left(\sum_\theta (A_\theta f_\theta) - d_0\right)\right\|_2^2 \\ & + \sum_\theta (\lambda_1 \|D_{1\theta} f_\theta\|_1 + \lambda_2 \|D_{2\theta} f_\theta\|_1) \\ & + \frac{\gamma}{2}\sum_\theta \left(\left\| H_{\Phi_\theta}\left(f_\theta - c_\theta \vec{1}\right)\right\|_2^2 + \left\|(I - H_{\Phi_\theta}) f_\theta\right\|_2^2\right), \\ & \text{subject to } f \geq 0, \end{aligned} \tag{3}$$

where I is the identity matrix, and H_{Φ_θ} in this notation is a diagonal matrix that has the information of $H(\Phi_\theta(x,y))$ along its diagonal for all x and y. Essentially, the diagonal of H_{Φ_θ} has a value of 1 if the corresponding $\Phi_\theta(x,y)$ is positive and zero otherwise. The formulation is solved using the Chambolle–Pock algorithm,[24] a proximal-class primal–dual algorithm. This algorithm solves the optimization problem in the form of

$$\text{minimize } S(Kx) + R(x). \tag{4}$$

S and R are lower semicontinuous functions, and K is a matrix. Equation (3) can be written in the form of Eq. (4) by defining

$$K = \begin{bmatrix} WA \\ D_1 \\ D_2 \\ H_\Phi \\ I - H_\Phi \end{bmatrix},$$

$$A = \begin{bmatrix} A_{\theta=1} & \cdots & A_{\theta=n} \end{bmatrix},$$

$$D_1 = \begin{bmatrix} D_{1\theta=1} & \cdots & 0 \\ \vdots & \ddots & \vdots \\ 0 & \cdots & D_{1\theta=n} \end{bmatrix},$$

$$D_2 = \begin{bmatrix} D_{2\theta=1} & \cdots & 0 \\ \vdots & \ddots & \vdots \\ 0 & \cdots & D_{2\theta=n} \end{bmatrix},$$

$$H_\Phi = \begin{bmatrix} H_{\Phi_{\theta=1}} & \cdots & 0 \\ \vdots & \ddots & \vdots \\ 0 & \cdots & H_{\Phi_{\theta=n}} \end{bmatrix},$$

$$f = \begin{bmatrix} f_{\theta=1} \\ \vdots \\ f_{\theta=n} \end{bmatrix} \qquad c = \begin{bmatrix} \vec{1}c_{\theta=1} \\ \vdots \\ \vec{1}c_{\theta=n} \end{bmatrix},$$

$$\begin{aligned} S(Kf) \;=\; & s_1(WAf) + s_2(D_1 f) + s_3(D_2 f) \\ & + s_4(H_\Phi f) + s_5((I - H_\Phi) f), \end{aligned}$$

$$R(f) = \begin{cases} 0 & \text{if } f \geq 0 \\ \infty & \text{otherwise} \end{cases}, \tag{5}$$

where

$$\begin{aligned} s_1(g_1) &= \frac{1}{2}\|g_1 - W d_0\|_2^2, \\ s_2(g_2) &= \lambda \|g_2\|_1, \\ s_3(g_3) &= \lambda \|g_3\|_1, \\ s_4(g_4) &= \frac{\gamma}{2}\|g_4 - H_\Phi c\|_2^2, \\ s_5(g_5) &= \frac{\gamma}{2}\|g_5\|_2^2. \end{aligned} \tag{6}$$

The overrelaxed Chambolle–Pock algorithm[25] is used to solve this formulation, with the iteration

$$\begin{aligned} \bar{f}^{n+1} &= \operatorname{prox}_{\tau R}\left(f^n - \tau K^T z^n\right), \\ \bar{z}^{n+1} &= \operatorname{prox}_{\sigma S^*}\left(z^n + \sigma K\left(2\bar{f}^{n+1} - f^n\right)\right), \\ f^{n+1} &= p\bar{f}^{n+1} + (1-p) f^n, \\ z^{n+1} &= p\bar{z}^{n+1} + (1-p) z^n. \end{aligned} \tag{7}$$

τ and σ are step sizes that satisfy the constraint $\tau\sigma\|K\|^2 \leq 1$, and p is the overrelaxation parameter ranging from 0 to 2. The operator norm of K is estimated with the power iteration method.[26] The proximity operator, or "prox" operator, is defined as $\operatorname{prox}_{th}(x) = \underset{u}{\operatorname{argmin}} \left(h(u) + 1/2t\|u - x\|_2^2\right)$, and S^* is the convex conjugate of S, defined as $S^*(z)$

$= \sup_y \left(z^T y - S(y)\right)$. Evaluation of these operations yield closed form, low cost calculations for the Chambolle–Pock algorithm,

$$\begin{aligned}
&\text{prox}_{\sigma s_1^*}(\widehat{z_1}) = \frac{\widehat{z_1} - \sigma W d_0}{1+\sigma},\\
&\text{prox}_{\sigma s_2^*}(\widehat{z_2}) = P_{\lambda B}(\widehat{z_2}),\\
&\text{prox}_{\sigma s_3^*}(\widehat{z_3}) = P_{\lambda B}(\widehat{z_3}),\\
&\text{prox}_{\sigma s_4^*}(\widehat{z_4}) = \gamma\left(\frac{\widehat{z_4} - \sigma H_\Phi c_\theta \bar{1}}{\gamma+\sigma}\right),\\
&\text{prox}_{\sigma s_4^*}(\widehat{z_5}) = \frac{\gamma \widehat{z_5}}{\gamma+\sigma},\\
&\text{prox}_{\tau R}(\hat{x}) = P_+(\hat{x}),
\end{aligned} \tag{8}$$

and a separable sum rule allows for

$$\text{prox}_{\sigma S^*}\left(\begin{bmatrix}\widehat{z_1}\\ \widehat{z_2}\\ \widehat{z_3}\\ \widehat{z_4}\\ \widehat{z_5}\end{bmatrix}\right) = \begin{bmatrix}\text{prox}_{\sigma s_1^*}(\widehat{z_1})\\ \text{prox}_{\sigma s_2^*}(\widehat{z_2})\\ \text{prox}_{\sigma s_3^*}(\widehat{z_3})\\ \text{prox}_{\sigma s_4^*}(\widehat{z_4})\\ \text{prox}_{\sigma s_5^*}(\widehat{z_5})\end{bmatrix}. \tag{9}$$

2.B.2. Algorithm module 2: Update c_θ

Step 2 minimizes Eq. (1) with respect to c_θ given Φ_θ and f_θ constant, which is provided by the closed-form solution

$$c_\theta = \frac{\sum_{x,y} f_{\theta xy} H(\Phi_\theta(x,y))}{\sum_{x,y} H(\Phi_\theta(x,y))} \quad \text{for } \theta = 1,\ldots,n. \tag{10}$$

This calculation takes an average of the beamlet intensities that are defined as part of the aperture for each beam angle.

2.B.3. Algorithm module 3: Update Φ_θ

Step 3 minimizes Eq. (1) with respect to Φ_θ while holding f_θ and c_θ constant,

$$\begin{aligned}
\underset{\{\Phi_\theta\}_{\theta=0}^n}{\text{argmin}} \sum_\theta \sum_{x,y} \Big(&\frac{\gamma}{2}\Big[\left(f_{\theta xy} - c_\theta\right)^2 H(\Phi_\theta(x,y))\\
&+ f_{\theta xy}^2 (1 - H(\Phi_\theta(x,y)))\Big]\\
&+ \frac{k}{2}\Big[\left(H(\Phi_\theta(x,y)) - H(\Phi_{\theta-1}(x,y))\right)^2\\
&+ \left(H(\Phi_\theta(x,y)) - H(\Phi_{\theta+1}(x,y))\right)^2\Big]\Big),
\end{aligned} \tag{11}$$

Φ_θ is iteratively updated by the expression

$$\Phi_\theta^{i+1}(x,y) = \Phi_\theta^i(x,y) + \frac{d\Phi_\theta^i(x,y)}{dt} dt, \tag{12}$$

where $\frac{d\Phi_\theta(x,y)}{dt}$ was derived as

$$\begin{aligned}
\frac{d\Phi_\theta(x,y)}{dt} = &\frac{\gamma}{2}\left(2c_\theta f_{\theta xy} - c_\theta^2\right)\delta(\Phi_\theta(x,y))dt\\
&+ k\left(H(\Phi_{\theta-1}(x,y)) + H(\Phi_{\theta+1}(x,y))\right.\\
&\left.- 2H(\Phi_\theta(x,y))\right)\delta(\Phi_\theta(x,y))dt.
\end{aligned} \tag{13}$$

The derivation for $\frac{d\Phi_\theta^i(x,y)}{dt}$ can be found in the appendix. Practically, we use the sigmoid function and its derivative to approximate the Heaviside and the Dirac delta function,

$$\begin{aligned}
&H(\Phi) \cong \text{Sigmoid}(q\Phi) = \frac{1}{1+e^{-q\Phi}},\\
&\delta(\Phi) = \frac{dH(\Phi)}{d\Phi} \cong \frac{d\text{Sigmoid}(q\Phi)}{d\Phi} = \frac{q e^{q\Phi}}{(1+e^{q\Phi})^2},
\end{aligned} \tag{14}$$

where q is some constant. A larger value of q allows for the sigmoid function to more closely resemble the Heaviside function.

2.B.4. Ensuring optimal plan quality

Once the algorithm has converged, and the apertures shapes no longer change, a final polishing step is taken to ensure superior plan quality. The formulation locks in the solved aperture shapes and solves for the fluence of each beam angle without the aperture regularization constraints,

$$\begin{aligned}
&\underset{b}{\text{argmin}} \quad \|W(AFb - d_0)\|_2^2,\\
&\text{subject to } b \geq 0,
\end{aligned} \tag{15}$$

The optimization variable, b, contains one intensity value for each beam angle. F is a binary matrix containing all of the aperture information from $H(\Phi_\theta(x,y))$ for all of the beam angles. These two variables are related to the fluence via the equation $f = Fb$. This optimization can be easily solved with the Chambolle–Pock algorithm. By solving the optimization in Eq. (15) as the last step, only the dose difference is penalized, ensuring that the regularization and aperture constraints are not hindering the final dosimetric outcome.

2.C. Evaluation

To assess the efficacy of the optimization, four patients were chosen for this study: A glioblastoma multiforme (GBM) patient, a lung (LNG) patient, and two head and neck patients, one with three PTVs ($H\&N_{3PTV}$) and one with four PTVs ($H\&N_{4PTV}$). Table I shows the four patients with their respective prescription doses and PTV volumes.

Using a convolution/superposition code with a 6 MV x-ray polyenergetic kernel, the beamlet dose was calculated for

TABLE I. Prescription doses and PTV volumes.

	Prescription dose (Gy)	PTV volume (cc)
GBM	25	6.23
LNG	50	47.78
$H\&N_{3PTV}$	54	197.54
	59.4	432.56
	69.96	254.98
$H\&N_{4PTV}$	54	58.98
	60	149.32
	66	242.23
	70	175.20

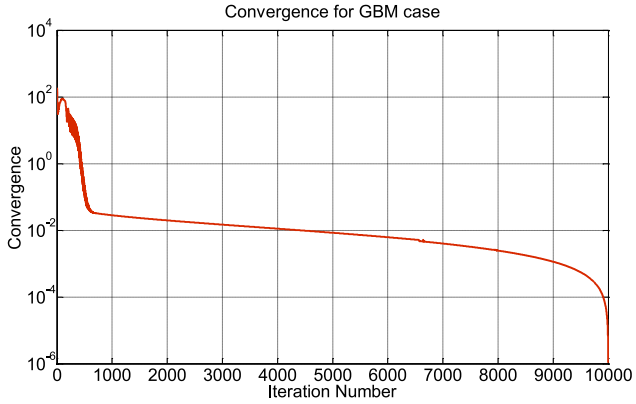

FIG. 1. Convergence plot for the GBM case. Convergence is defined as convergence(k) = (objval(k) − minobj)/minobj, where objval(k) is the objective value at the kth iteration and minobj is the minimum objective value, taken at the 10 000th iteration. Objective value is based off of the objective function defined in Eq. (1) and is recorded after each block iteration of modules 1, 2, and 3.

180 equally spaced coplanar beam angles around the patient. The dose calculation method was described in our previous publications.[27,28] The chosen beamlet size was 0.5×0.5 cm^2, and the dose matrix resolution was $0.25\times0.25\times0.25$ cm^3. The resulting dose was stored in the dose matrix A for optimization. A 5 cm ring structure was added to the optimization to minimize dose spillage. Each patient was then optimized using the comVMAT algorithm, and W was adjusted until a desirable dose was achieved.

The comVMAT plans were compared to the patients' respective clinical VMAT plan (clnVMAT). The clnVMAT plans were planned on the Eclipse treatment planning system using two superimposing 360° coplanar arcs with 90° collimator rotation. The PTV $D95$, $D98$, $D99$, Dmax, and PTV homogeneity, defined as $D95/D5$, were evaluated. The organs-at-risk (OARs) Dmax and Dmean were also assessed. Max dose is defined as the dose at 2% of the structure volume, $D2$, which is recommended by the ICRU-83 report.[29]

3. RESULTS

The aperture shapes converged, with a relative convergence of 10^{-1}, within 600 iterations of the optimization for each case. This degree of convergence has been shown to produce plans that are dosimetrically equivalent to other plans that have tighter convergences.[22] A convergence plot for the GBM case is shown in Fig. 1, showing the convergence relative to the optimal value taken at the 10 000th iteration. The oscillatory convergence pattern in the beginning before 600 iterations comes from the alternating optimizations to solve for f, c, and Φ. The variables are each taking small steps toward optimality, but may make the other variables temporarily and slightly less optimal in a given iteration. However this pattern diminishes after 600 iterations. Depending on various factors—such as case complexity, tumor volume, and body volume—total computational time varied from 5 min for the GBM case to 40 min for the H&N cases, per optimization run. Unlike the clinical implementation, no human involvement is required during the optimization process after the weights have been set. While the overall planning time is within acceptable range, the algorithm was written and tested in MATLAB for proof of principle. Its performance should improve considerably using faster programming language.

The comVMAT method managed to optimize all 180 beams in the coplanar arc simultaneously for all tested cases. Figure 2 shows the 180 apertures from the GBM case. The MLC leaf motion direction is horizontal in the schematic. It is observed that beam aperture shapes are similar to their neighbors. A small fraction of beams, such as beam 3 and beam 26, require two segments to deliver. Since every beam is spaced apart by 2°, in practice, these beams can be split into two beams spaced 1° apart, each delivering one of the apertures. The gantry speed may be modulated in order to deliver the apertures.

Figure 3 shows the 4 DVHs from each of the patients, comparing the comVMAT plans against the clnVMAT plans. Qualitatively, it can be observed that comVMAT is able to better spare the OARs while maintaining a competitive PTV dosimetry. The two H&N cases with multiple PTVs, while matching the dose coverage to 95% of the PTVs, had slightly hotter tails to the PTVs by a few Gy with the comVMAT plan. PTVs are shown in green shades for the H&N$_{3\text{PTV}}$ case and blue shades for the H&N$_{4\text{PTV}}$ case in Fig. 3. However this marginal increase is outweighed by the substantial sparing in all of the OARs for each plan. The GBM and LNG cases, which had only 1 PTV, were superior in all aspects with the comVMAT plans (Table II).

On average, the PTV $D95$, $D98$, and $D99$ changed by −0.01%, +0.02%, and −0.23% of the prescription dose, indicating virtually identical dose coverage between comVMAT and clnVMAT. However PTV Dmax increased, on average, by 1.40% of the prescription dose. This change is associated to the two H&N cases with multiple PTVs. The GBM case actually had reduced max dose to the PTV, while the LNG case minimally increased the PTV max dose by 0.08% of the prescription dose. The average calculations include all of the PTVs from the H&N cases. The comVMAT optimizer was able to decrease all of the OARs from all of the cases, shown in Table III, where the largest valued dose differences were still negative. On average, comVMAT plan spared the OARs max and mean dose by 6.59% and 7.45% of the prescription dose, respectively. Comparing all the cases, the LNG case had the single largest sparing in max dose in an OAR, and spared the proximal bronchus by 14.5 Gy of max dose. Likewise, the single largest reduction in the mean dose to an OAR was from the H&N$_{3\text{PTV}}$ case, sparing the larynx by 15.3 Gy of mean dose.

Figure 4 shows the dose wash for all of the patients. From a qualitative perspective, it can be observed that comVMAT distributes the dose very differently than clnVMAT. The GBM and LNG cases more clearly illustrate that comVMAT plans gave a much heavier weighting to some selective beams, giving rise to a dose distribution that bears some resemblance to a coplanar IMRT plan, even though there is still only 1 fluence value per beam angle. The clnVMAT overall spreads the distribution of fluence intensities more evenly among the beams, giving rise to a less angular modulated dose

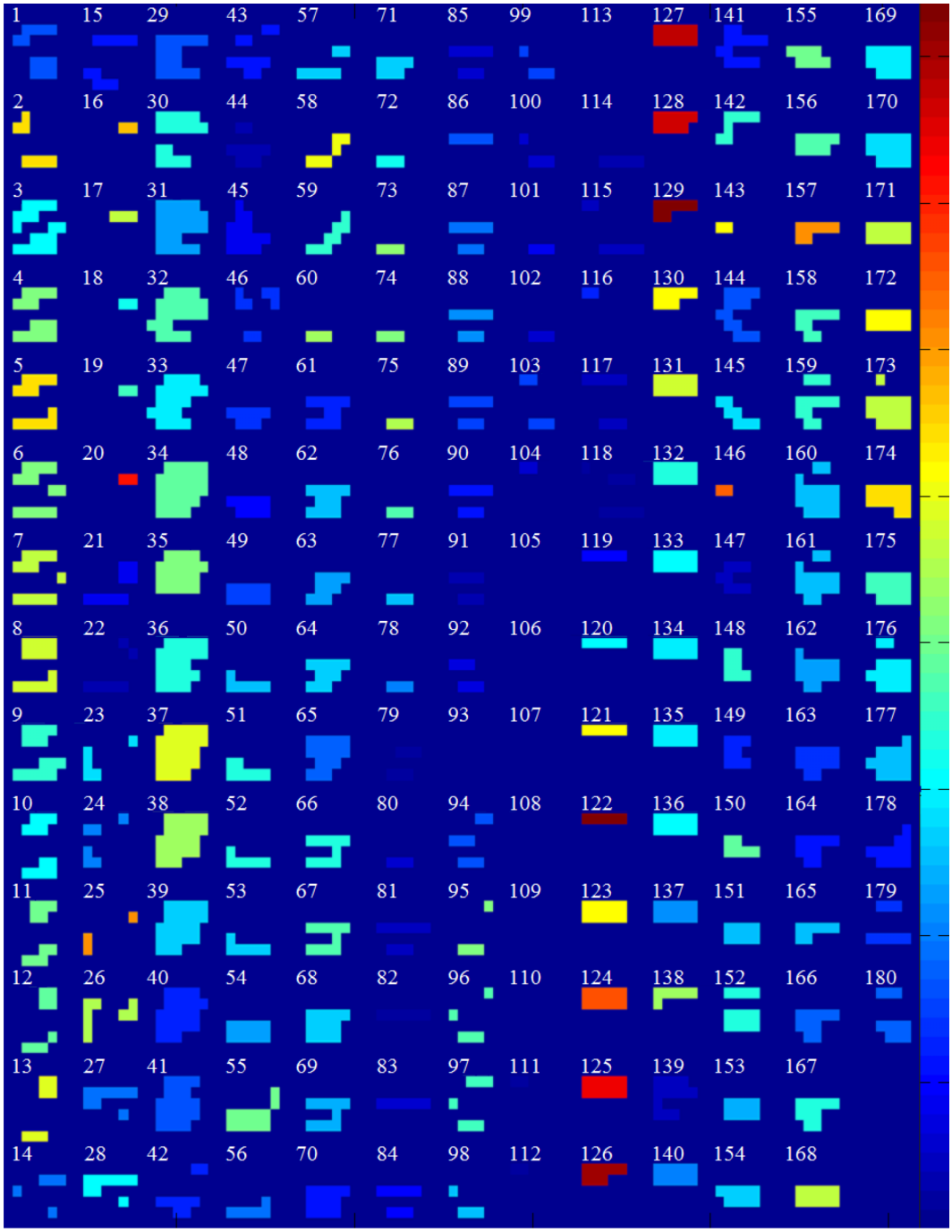

FIG. 2. Schematic of apertures for all 180 beams, spaced 2° apart, for GBM case. MLC leaf direction is horizontal for this diagram. Color scales show fluence intensities.

distribution pattern and greater dose to OARs. For example, for the GBM plan in Fig. 3, the comVMAT plan was able to entirely avoid the brainstem, while the clnVMAT plan covers the brainstem with at least 2.5 Gy of dose.

4. DISCUSSION

When solved using an algorithm based on a proximal-class primal–dual algorithm, the Chambolle–Pock algorithm,[24] we found a new methods, based on L2-norm fidelity terms and L1-norm regularization terms,[22,30] to incorporate fluence maps simplification into the dose domain optimization. In this study, we further developed the methods to solve the VMAT problem, which previously only had greedy heuristic solutions. The new method optimizes all VMAT beams at the same time without progressive sampling. This translates into a number of theoretical and practical advantages.

At the theoretical level, the optimization cost function provides a simple yet complete description of the physical problem. An L2-norm fidelity term is used to minimize the dose distribution of the prescription dose, and an anisotropic total variation regularization term to piecewise smooth the

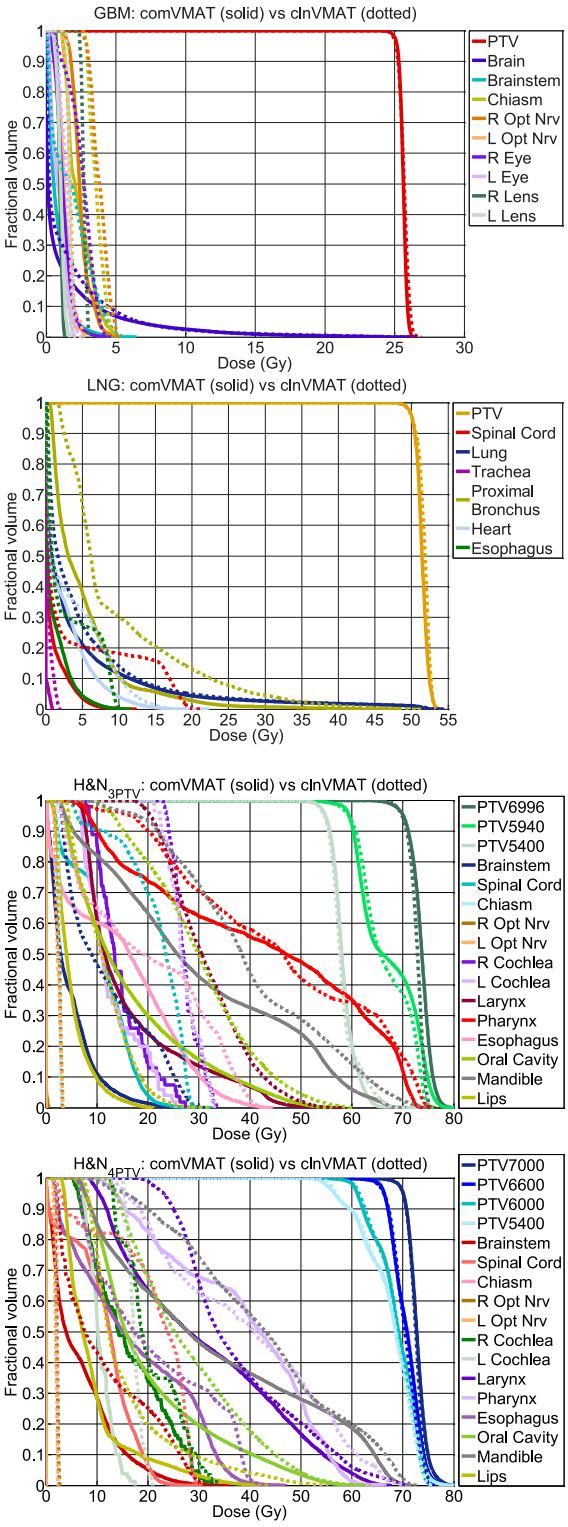

FIG. 3. DVHs of the GBM, LNG, H&N$_{3PTV}$, and H&N$_{4PTV}$ patients comparing the comVMAT and clnVMAT plans.

fluence map. The following level set function term shapes the fluence to fit the aperture and then encourages the continuity in the aperture shapes between adjacent beams. As we demonstrated, solving the optimization problem results in a final solution that requires no additional "patches" that are commonly observed in heuristic solutions. Because of the optimization problem size and the fact that the cost function is not differentiable, methods such as interior points and gradient descent are not suitable to solve the optimization problem. We instead used the Chambolle–Pock algorithm[24] to efficiently manage the optimization problem. The algorithm is remarkably fast at solving this type of optimization problem because it does not require solving system of linear equations involving the fluence to dose transformation matrix, A, at every iteration, unlike other first order methods such as alternating direction method of multipliers.[31] Instead, Chambolle–Pock simply requires just the multiplication of the matrix and its transpose at each iteration.

The comVMAT method is superior to existing VMAT methods in the following aspects. comVMAT optimizes all beam apertures and beam intensities together, providing greater flexibility to approach the ideal dose. A difference in isodose distribution can be appreciated in Fig. 4, where clnVMAT resulted in a more uniform dose spillage and comVMAT gave heavy weights to a narrow range of beams, resulting in dose distribution resembling beam orientation optimized static beam IMRT or hybrid IMRT VMAT plans.[32] In terms of the optimization solver, the analytical solution used in comVMAT is more robust that the stochastic or greedy heuristic algorithms used in existing VMAT methods. Moreover, comVMAT solves the direct aperture problem. Previously, the aperture was generated either in an additional step that degraded the optimization results, or was limited to use a small subset of available apertures[33,34] due to nonpolynomial computational cost to include all possible apertures. In contrast, comVMAT can arrive at any aperture shape without being limited to a preset library or the neighborhood of conformal apertures.

A remaining issue in comVMAT is that the resultant aperture per beam is not explicitly guaranteed to be deliverable in one segment. While the total variation regularization term has limited the number of apertures for most beams to 1, there are a small fraction of beams that require more apertures. For example, in Fig. 2, beams 3, 26, and 46 have segments that must be delivered in two apertures. While increasing the regularization weighting may eliminate multiple apertures

TABLE II. PTV homogeneity, dose coverage ($D95$, $D98$, and $D99$), and Dmax.

		PTV statistics					
		Homogeneity		$D95$	$D98$	$D99$	Dmax
Patient case		comVMAT	clnVMAT	comVMAT − clnVMAT (Gy)			
GBM		0.968	0.958	+0.08	+0.09	+0.02	−0.21
LNG		0.949	0.948	+0.00	+0.13	+0.09	+0.04
H&N$_{3PTV}$	54	0.874	0.847	+0.23	+0.19	+0.06	−2.30
	59.4	0.786	0.801	+0.02	+0.73	+0.15	+1.96
	69.96	0.915	0.935	+0.29	−0.12	−0.63	+2.36
H&N$_{4PTV}$	54	0.760	0.771	−0.30	−0.97	−1.06	+1.11
	60	0.818	0.832	−0.40	−0.18	−0.11	+1.17
	66	0.885	0.895	+0.05	+0.36	+0.26	+1.40
	70	0.924	0.940	+0.00	−0.05	−0.10	+2.08

TABLE III. Largest, smallest, and average values found for (comVMAT − clnVMAT) dose differences for *D*max and *D*mean.

Dose difference comVMAT – clnVMAT (Gy)	*D*max			*D*mean		
	Largest value	Smallest value	Average value	Largest value	Smallest value	Average value
GBM	−0.02 Chiasm	−1.76 R Lens	−0.80	−0.43 L Opt Nrv	−1.73 R Lens	−1.04
LNG	−0.38 Lung	−14.53 ProxBronch	−5.63	−0.37 Trachea	−4.61 ProxBronch	−1.98
$H\&N_{3PTV}$	−1.95 Pharynx	−9.74 Brainstem	−4.91	−2.43 R Opt Nrv	−15.31 Larynx	−8.26
$H\&N_{4PTV}$	−0.56 OralCavity	−13.38 Lips	−4.33	−1.16 Pharynx	−9.47 Mandible	−5.13

per beam, there may be a compromise in the dosimetry if the TV penalty is too high. There are multiple solutions in handling the delivery of these particular beams. Since each aperture delivery is spread across 2°, the first solution is to split the beam into two 1°-apart beams and deliver the two segments sequentially. Alternatively, the two segments may be approximated by the closest single segment. The alternative would result in change in dose distribution but the change is expected to be minimal because only a small fraction of beams need more than 1 MLC segment. On the other hand, the issue may become an opportunity for generating hybrid static beam IMRT and VMAT plans. By further relaxing the TV regularization, we expect dosimetric improvement and more beams that require two or more MLC segments. The gantry speed and Linac output would be modulated to deliver these beams, adding more static beam flavor to comVMAT for superior dosimetry.

Delivery time of the plans is not explicitly controlled by the objective function, but instead is indirectly maintained by the total variation term, term set 1, to limit the number of deliverable segments, and the aperture similarity term, term set 3, to limit the MLC leaf motion between each angle. Relaxing the weights on these terms to allow more segments and greater changes between apertures will increase treatment time and offset the benefit of using a single arc. The trade-off between plan quality and delivery time is a topic of further investigation.

At the practical level, the single arc comVMAT is shown superior to the current commercial implementation of clnVMAT using two superimposing arcs. comVMAT may be potentially advantageous, pending further research, in knowledge based planning because it is more robust to the optimization history, while clnVMAT depends on the entire history of optimization parameter set up, which is impossible to track and incorporate in knowledge based planning. The comVMAT plans are reproducible, providing a single set of optimization parameters for future learning.

The focus of the study is to present a new VMAT formulism that does not depend on greedy heuristics and results in dosimetry that is at least comparable to the multiple arc VMAT plans using a single arc. While we have carefully fine-tuned our dose calculation code to match the PDD and penumbra of the Eclipse system beams, the TPC commissioning process is not entirely transparent for us to exactly reproduce. The TPS vendor will have to implement our algorithm for an exact comparison.

As a VMAT approach, the particular DAO formulation that was presented was specifically tailored to produce one segment per beam in most cases. Generalization of the method for applications including static beam IMRT requires multiple level of segmentation that requires different mathematical tools. We will explore the potential of an approach to a generalized libraryless DAO formulation for both static beam and VMAT IMRT problems.

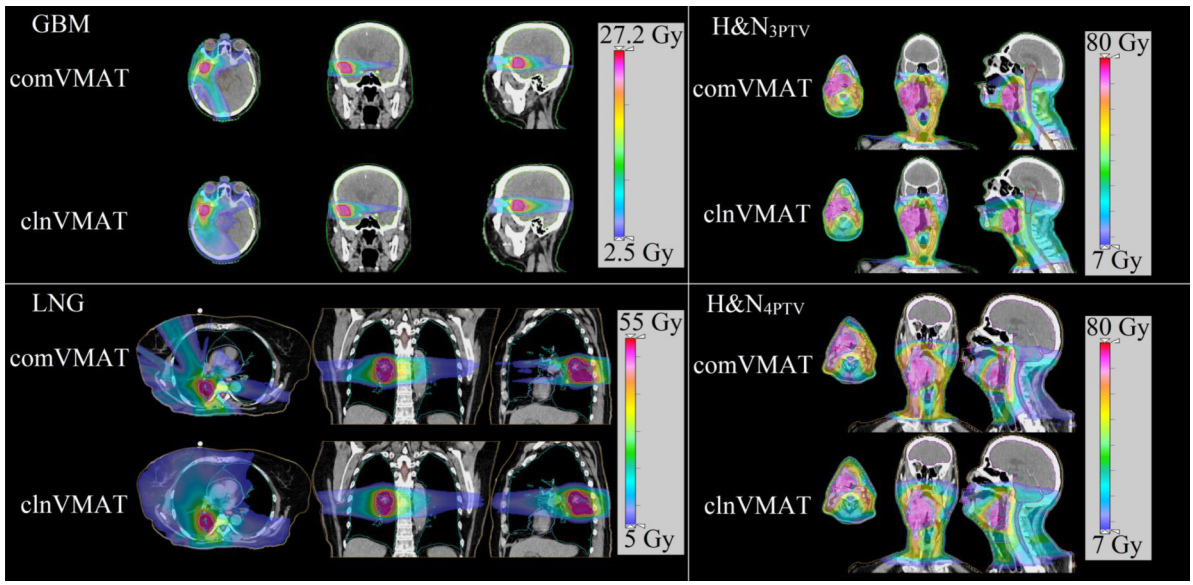

FIG. 4. Dose washes for all patients. The low dose cutoff for viewing is set at 10% of the prescription dose.

5. CONCLUSION

A new approach for the comprehensive VMAT optimization was demonstrated. The new approach formulates the VMAT problem as a single optimization function, including a level set function to regularize the MLC aperture shapes without relying on a preset aperture library. The optimization function was solved using a proximal-class primal–dual algorithm, which is more robust than stochastic method used in the existing VMAT solutions. The results showed that the new comVMAT using a single arc was consistently superior in OAR sparing to the clinical VMAT using two arcs, while keeping a similar PTV dosimetry. The comVMAT expression was a specialized form of a DAO that aims at reducing the number of segments per beam to exactly 1. Generalization of an approach to a libraryless DAO has yet to be fully explored.

ACKNOWLEDGMENTS

This research is supported in part by Varian Medical Systems, Inc., and NIH Grant Nos. R43CA183390 and R01CA188300.

CONFLICT OF INTEREST DISCLOSURE

The authors have no COI to report.

APPENDIX: DERIVATION OF $d\Phi_\theta(x,y)/dt$

Equation (11) can be first written as

$$\sum_\theta \sum_{x,y} \left(\frac{\gamma}{2} \left[(f_{\theta xy} - c_\theta)^2 H(\Phi_\theta(x,y)) + f_{\theta xy}^2 (1 - H(\Phi_\theta(x,y))) \right] + \frac{k}{2} \left[2H(\Phi_\theta(x,y))^2 - 2(H(\Phi_{\theta-1}(x,y)) + H(\Phi_{\theta+1}(x,y)))H(\Phi_\theta(x,y)) + H(\Phi_{\theta-1}(x,y))^2 + H(\Phi_{\theta+1}(x,y))^2 \right] \right). \quad \text{(A1)}$$

The formulation can be solved using gradient descent, where Φ_θ can be updated by the equation.

To iteratively determine Φ_θ, we change Φ_θ by a small step $d\Phi_\theta(x,y)/dt$, which changes Eq. (A1) to

$$\sum_\theta \sum_{x,y} \left(\frac{\gamma}{2} \left[(f_{\theta xy} - c_\theta)^2 H\left(\Phi_\theta(x,y) + \frac{d\Phi_\theta(x,y)}{dt} dt\right) - f_{\theta xy}^2 H\left(\Phi_\theta(x,y) + \frac{d\Phi_\theta(x,y)}{dt} dt\right) + f_{\theta xy}^2 \right] + \frac{k}{2} \left[2H\left(\Phi_\theta(x,y) + \frac{d\Phi_\theta(x,y)}{dt} dt\right)^2 - 2(H(\Phi_{\theta-1}(x,y)) + H(\Phi_{\theta+1}(x,y)))H\left(\Phi_\theta(x,y) + \frac{d\Phi_\theta(x,y)}{dt} dt\right) + H(\Phi_{\theta-1}(x,y))^2 + H(\Phi_{\theta+1}(x,y))^2 \right] \right). \quad \text{(A2)}$$

The first order Taylor expansion of Eq. (A2) is

$$\sum_\theta \sum_{x,y} \left(\frac{\gamma}{2} \left[(f_{\theta xy} - c_\theta)^2 \left(H(\Phi_\theta(x,y)) + \delta(\Phi_\theta(x,y)) \frac{d\Phi_\theta(x,y)}{dt} dt \right) - f_{\theta xy}^2 \left(H(\Phi_\theta(x,y)) + \delta(\Phi_\theta(x,y)) \frac{d\Phi_\theta(x,y)}{dt} dt \right) + f_{\theta xy}^2 \right] + \frac{k}{2} \left[2 \left(H(\Phi_\theta(x,y))^2 + 2H(\Phi_\theta(x,y)) \delta(\Phi_\theta(x,y)) \frac{d\Phi_\theta(x,y)}{dt} dt \right) - 2(H(\Phi_{\theta-1}(x,y)) + H(\Phi_{\theta+1}(x,y))) \left(H(\Phi_\theta(x,y)) + \delta(\Phi_\theta(x,y)) \frac{d\Phi_\theta(x,y)}{dt} dt \right) + H(\Phi_{\theta-1}(x,y))^2 + H(\Phi_{\theta+1}(x,y))^2 \right] \right). \quad \text{(A3)}$$

Gathering all of the terms that include $d\Phi_\theta(x,y)/dt$ results in

$$\sum_\theta \sum_{x,y} \left(\frac{\gamma}{2} \left[(f_{\theta xy} - c_\theta)^2 - f_{\theta xy}^2 \right] + \frac{k}{2} [4H(\Phi_\theta(x,y)) - 2(H(\Phi_{\theta-1}(x,y)) + H(\Phi_{\theta+1}(x,y)))] \right) \delta(\Phi_\theta(x,y)) \frac{d\Phi_\theta(x,y)}{dt} dt + \frac{\gamma}{2} \left[(f_{\theta xy} - c_\theta)^2 H(\Phi_\theta(x,y)) - f_{\theta xy}^2 H(\Phi_\theta(x,y)) + f_{\theta xy}^2 \right] + \frac{k}{2} \left[2H(\Phi_\theta(x,y))^2 - 2(H(\Phi_{\theta-1}(x,y)) + H(\Phi_{\theta+1}(x,y)))H(\Phi_\theta(x,y)) + H(\Phi_{\theta-1}(x,y))^2 + H(\Phi_{\theta+1}(x,y))^2 \right]. \quad \text{(A4)}$$

Simplifying the Eq. (A4) yields

$$\sum_\theta \sum_{x,y} \left[\frac{\gamma}{2} (c_\theta^2 - 2c_\theta f_{\theta xy}) + k(2H(\Phi_\theta(x,y)) - H(\Phi_{\theta-1}(x,y)) - H(\Phi_{\theta+1}(x,y))) \right] \delta(\Phi_\theta(x,y)) \frac{d\Phi_\theta(x,y)}{dt} dt + \frac{\gamma}{2} \left[(c_\theta^2 - 2c_\theta f_{\theta xy}) H(\Phi_\theta(x,y)) + f_{\theta xy}^2 \right] + \frac{k}{2} \left[(H(\Phi_\theta(x,y)) - H(\Phi_{\theta-1}(x,y)))^2 + (H(\Phi_\theta(x,y)) - H(\Phi_{\theta+1}(x,y)))^2 \right]. \quad \text{(A5)}$$

The first set of terms that include $d\Phi_\theta(x,y)/dt$ can be rewritten as the inner product

$$\begin{aligned}\sum_\theta \sum_{x,y} \Big[&\frac{\gamma}{2}\left(c_\theta^2 - 2c_\theta f_{\theta xy}\right) + k\left(2H(\Phi_\theta(x,y)) - H(\Phi_{\theta-1}(x,y))\right.\\ &\left. - H(\Phi_{\theta+1}(x,y))\right)]\delta(\Phi_\theta(x,y))dt, \frac{d\Phi_\theta(x,y)}{dt}\\ &+\frac{\gamma}{2}\left[\left(c_\theta^2 - 2c_\theta f_{\theta xy}\right)H(\Phi_\theta(x,y)) + f_{\theta xy}^2\right]\\ &+\frac{k}{2}\left[\left(H(\Phi_\theta(x,y)) - H(\Phi_{\theta-1}(x,y))\right)^2\right.\\ &\left.+\left(H(\Phi_\theta(x,y)) - H(\Phi_{\theta+1}(x,y))\right)^2\right]. \qquad \text{(A6)}\end{aligned}$$

The terms $f_{\theta xy}$, c_θ, Φ_θ, $\Phi_{\theta-1}$, and $\Phi_{\theta+1}$ are treated as constants while solving for $d\Phi_\theta(x,y)/dt$. Hence, we only need to consider the terms that have $d\Phi_\theta(x,y)/dt$. It is easy to see that the minimizer of Eq. (A6) is when

$$\begin{aligned}\frac{d\Phi_\theta(x,y)}{dt} = &\frac{\gamma}{2}\left(2c_\theta f_{\theta xy} - c_\theta^2\right)\delta(\Phi_\theta(x,y))dt\\ &+ k\left(H(\Phi_{\theta-1}(x,y)) + H(\Phi_{\theta+1}(x,y))\right.\\ &\left.- 2H(\Phi_\theta(x,y))\right)\delta(\Phi_\theta(x,y))dt. \qquad \text{(A7)}\end{aligned}$$

[a]Author to whom correspondence should be addressed. Electronic mail: ksheng@mednet.ucla.edu

[1]W. F. A. R. Verbakel, J. P. Cuijpers, D. Hoffmans, M. Bieker, B. J. Slotman, and S. Senan, "Volumetric intensity-modulated arc therapy vs conventional IMRT in head-and-neck cancer: A comparative planning and dosimetric study," Int. J. Radiat. Oncol., Biol., Phys. **74**, 252–259 (2009).

[2]M. Kawashima, S. Ozawa, A. Haga, A. Sakumi, C. Kurokawa, S. Sugimoto, K. Karasawa, K. Nakagawa, and K. Sasai, "Comparison of total MU and segment areas in VMAT and step-and-shoot IMRT plans," Radiol. Phys. Technol. **6**, 14–20 (2013).

[3]M. Rao, W. Yang, F. Chen, K. Sheng, J. Ye, V. Mehta, D. Shepard, and D. Cao, "Comparison of Elekta VMAT with helical tomotherapy and fixed field IMRT: Plan quality, delivery efficiency and accuracy," Med. Phys. **37**, 1350–1359 (2010).

[4]J. L. Bedford, "Treatment planning for volumetric modulated arc therapy," Med. Phys. **36**, 5128–5138 (2009).

[5]C. X. Yu, "Intensity-modulated arc therapy with dynamic multileaf collimation: An alternative to tomotherapy," Phys. Med. Biol. **40**, 1435–1449 (1995).

[6]D. M. Shepard, D. Cao, M. K. N. Afghan, and M. A. Earl, "An arc-sequencing algorithm for intensity modulated arc therapy," Med. Phys. **34**, 464–470 (2007).

[7]M. Earl, D. Shepard, S. Naqvi, X. Li, and C. Yu, "Inverse planning for intensity-modulated arc therapy using direct aperture optimization," Phys. Med. Biol. **48**, 1075–1089 (2003).

[8]J.-Y. Jin, N. Wen, L. Ren, C. Glide-Hurst, and I. J. Chetty, "Advances in treatment techniques: Arc-based and other intensity modulated therapies," Cancer J. **17**, 166–176 (2011).

[9]S. M. Crooks, X. Wu, C. Takita, M. Watzich, and L. Xing, "Aperture modulated arc therapy," Phys. Med. Biol. **48**, 1333–1344 (2003).

[10]K. Bratengeier, "2-Step IMAT and 2-Step IMRT in three dimensions," Med. Phys. **32**, 3849–3861 (2005).

[11]D. Cao, M. K. Afghan, J. Ye, F. Chen, and D. M. Shepard, "A generalized inverse planning tool for volumetric-modulated arc therapy," Phys. Med. Biol. **54**, 6725–6738 (2009).

[12]K. Otto, "Volumetric modulated arc therapy: IMRT in a single gantry arc," Med. Phys. **35**, 310–317 (2008).

[13]T. Bortfeld and S. Webb, "Single-arc IMRT?," Phys. Med. Biol. **54**, N9–N20 (2009).

[14]D. Craft, D. McQuaid, J. Wala, W. Chen, E. Salari, and T. Bortfeld, "Multi-criteria VMAT optimization," Med. Phys. **39**, 686–696 (2012).

[15]S. Luan, C. Wang, D. Z. Chen, X. S. Hu, S. A. Naqvi, C. X. Yu, and C. L. Lee, "A new MLC segmentation algorithm/software for step-and-shoot IMRT delivery," Med. Phys. **31**, 695–707 (2004).

[16]P. Xia, A. B. Hwang, and L. J. Verhey, "A leaf sequencing algorithm to enlarge treatment field length in IMRT," Med. Phys. **29**, 991–998 (2002).

[17]W. Que, "Comparison of algorithms for multileaf collimator field segmentation," Med. Phys. **26**, 2390–2396 (1999).

[18]F. Peng, X. Jia, X. Gu, M. A. Epelman, H. E. Romeijn, and S. B. Jiang, "A new column-generation-based algorithm for VMAT treatment plan optimization," Phys. Med. Biol. **57**, 4569–4588 (2012).

[19]L.-T. Cheng, B. Dong, C. Men, X. Jia, and S. Jiang, "Binary level-set shape optimization model and algorithm for volumetric modulated arc therapy in radiotherapy treatment," SIAM J. Sci. Comput. **35**, B1321–B1340 (2013).

[20]S. Osher and R. Fedkiw, *Level Set Methods and Dynamic Implicit Surfaces* (Springer Science & Business Media, New York, 2006).

[21]L. Zhu, L. Lee, Y. Ma, Y. Ye, R. Mazzeo, and L. Xing, "Using total-variation regularization for intensity modulated radiation therapy inverse planning with field-specific numbers of segments," Phys. Med. Biol. **53**, 6653–6672 (2008).

[22]D. Nguyen, D. O'Connor, V. Y. Yu, D. Ruan, M. Cao, D. A. Low, and K. Sheng, "Dose domain regularization of MLC leaf patterns for highly complex IMRT plans," Med. Phys. **42**, 1858–1870 (2015).

[23]J. Gorski, F. Pfeuffer, and K. Klamroth, "Biconvex sets and optimization with biconvex functions: A survey and extensions," Math. Methods Oper. Res. **66**, 373–407 (2007).

[24]A. Chambolle and T. Pock, "A first-order primal–dual algorithm for convex problems with applications to imaging," J. Math. Imaging Vision **40**, 120–145 (2011).

[25]L. Condat, "A primal–dual splitting method for convex optimization involving Lipschitzian, proximable and linear composite terms," J. Optim. Theory Appl. **158**, 460–479 (2013).

[26]G. H. Golub and C. F. Van Loan, *Matrix Computations* (Johns Hopkins University, Baltimore, London, 1989).

[27]J. Neylon, K. Sheng, V. Yu, Q. Chen, D. A. Low, P. Kupelian, and A. Santhanam, "A nonvoxel-based dose convolution/superposition algorithm optimized for scalable GPU architectures," Med. Phys. **41**, 101711 (15pp.) (2014).

[28]P. Dong, P. Lee, D. Ruan, T. Long, E. Romeijn, D. A. Low, P. Kupelian, J. Abraham, Y. Yang, and K. Sheng, "4pi noncoplanar stereotactic body radiation therapy for centrally located or larger lung tumors," Int. J. Radiat. Oncol., Biol., Phys. **86**, 407–413 (2013).

[29]V. Grégoire and T. R. Mackie, "State of the art on dose prescription, reporting and recording in Intensity-Modulated Radiation Therapy (ICRU report No. 83)," Cancer/Radiothér. **15**, 555–559 (2011).

[30]D. Nguyen, D. Ruan, D. O'Connor, K. Woods, D. A. Low, S. Boucher, and K. Sheng, "A novel software and conceptual design of the hardware platform for intensity modulated radiation therapy," Med. Phys. **43**, 917–929 (2016).

[31]S. Boyd, in *Presented at the Talk at NIPS Workshop on Optimization and Machine Learning* (2011).

[32]H. Kim, R. Li, R. Lee, T. Goldstein, S. Boyd, E. Candes, and L. Xing, "Dose optimization with first-order total-variation minimization for dense angularly sampled and sparse intensity modulated radiation therapy (DASSIM-RT)," Med. Phys. **39**, 4316–4327 (2012).

[33]C. Men, H. E. Romeijn, Z. C. Taşkın, and J. F. Dempsey, "An exact approach to direct aperture optimization in IMRT treatment planning," Phys. Med. Biol. **52**, 7333–7352 (2007).

[34]E. Salari and J. Unkelbach, "A column-generation-based method for multi-criteria direct aperture optimization," Phys. Med. Biol. **58**, 621–639 (2013).